

PAIN Publish Ahead of Print
DOI: 10.1097/j.pain.0000000000001837

Peripheral and central nervous system alterations in a rat model of inflammatory arthritis

Samantha Locke^{1,3}, Noosha Yousefpour^{1,3}, Matthew Mannarino¹, Shuran Xing¹, Fatima Yashmin¹, Valerie Bourassa^{1,3} and Alfredo-Ribeiro-da-Silva^{1,2,3}

¹Department of Pharmacology and Therapeutics, McGill University, Montreal, Quebec, H3G 1Y6, Canada

²Department of Anatomy and Cell Biology, McGill University, Montreal, Quebec, H3A 2B2, Canada

³Alan Edwards Center for Research on Pain, McGill University, Montreal, Quebec H3A 0G1

Correspondence to: Dr. Alfredo Ribeiro-da-Silva, Department of Pharmacology and Therapeutics, 12 McGill University, 3655 Promenade Sir William-Osler, Montreal, Quebec, Canada H3G 1Y6. E-mail: alfredo.ribeirodasilva@mcgill.ca

Number of pages: 37

Number of figures: 9

Number of words: abstract (248), introduction (476) and discussion (1446)

None of the authors has conflicts of interest to disclose.

Abstract

It is consistently reported that in inflammatory arthritis (IA) pain may continue despite well controlled inflammation, most likely due to interactions between joint pathology and pain pathway alterations. Nervous system alterations have been described but much remains to be understood about neuronal and central non-neuronal changes in inflammatory arthritis.

Using a rat model of IA induced by intra-articular CFA injection, this study includes a thorough characterization of joint pathology, and objectives to identify peripheral innervation changes and alterations in the spinal dorsal horn (DH) that could alter DH excitatory balancing. Male and female rats displayed long-lasting pain-related behavior but, in agreement with our previous studies, other pathological alterations emerged only at later times. Cartilage vascularization, thinning and decreased proteoglycan content were not detectable in the ipsilateral cartilage until 4 weeks post-CFA. Sympathetic and peptidergic nociceptive fibers invaded the ipsilateral cartilage alongside blood vessels, complex innervation changes were observed in the surrounding skin and ipsilateral NGF protein expression was increased. In the DH, we examined innervation by peptidergic and non-peptidergic nociceptors, inhibitory terminal density, the K-Cl co-transporter KCC2, microgliosis and astrocytosis. Here, we detected the presence of microgliosis and interestingly, an apparent loss of inhibitory terminals and decreased expression of KCC2.

In conclusion, we found evidence of anatomical, inflammatory and neuronal alterations in the peripheral and central nervous systems in a model of inflammatory arthritis. Together these suggest that there may be a shift in the balance between incoming and outgoing excitation, and modulatory inhibitory tone in the DH.

Keywords: joint pain; intra-articular CFA; behaviour; Spinal cord; disinhibition; sprouting; peptidergic afferents; sympathetic; KCC2; microglia; NGF; western blot; Immunohistochemistry

Introduction

Arthritis, an umbrella term for a group of joint diseases, involves joint pain, inflammation and degradation. Unfortunately, pain in inflammatory arthritis (IA) may continue even when treatment with biologics has successfully controlled inflammation [41], suggesting the presence of mechanisms besides joint inflammation. A major hurdle hindering the development of mechanistically targeted treatments for IA pain is that the mechanisms of joint pain are poorly understood [57]. Patients often report to the clinic with advanced disease, which leaves gaining insight into development, progression and maintenance of pain in arthritis difficult from clinical studies alone. Following arthritis pathogenesis over time in animal models, such as the intra-articular Complete Freund's Adjuvant (CFA) model (IA-CFA model), can offer insight into mechanisms of joint pain [7]. Pathological joint alterations that reproduce clinical observations have been demonstrated in this model [7; 29], however almost no studies provide quantitative data on when such changes occur.

In IA, pathology is not restricted to the joint; alterations to the peripheral [1; 22; 60] and central nervous systems (CNS) [2; 39; 51] have been demonstrated in pre-clinical and clinical studies [21; 56]. In the periphery, nociceptors [13; 26] and mechanoreceptors [31] can become sensitized and nerve fiber sprouting has been described [1; 22; 37], in addition to sensitization in the CNS [reviewed in 43]. Previously, we have demonstrated sympathetic fiber sprouting and a role for the sympathetic system in pain in a similar IA-CFA model at 4-weeks post-CFA only [37]. Ours

and other studies [30; 44] highlight that some changes may not emerge until later time-points in models of arthritis. This is particularly important as the mechanisms underlying pain in early and late clinical disease [23; 58; 59], or those in play during persistent vs resolved inflammation [41], may vary.

The first main aims of this study were to provide a thorough characterization of joint pathology and peripheral innervation changes in the IA-CFA model, and to confirm that findings previously identified in males also occur in females. As the spinal dorsal horn (DH) is the first site in the CNS where nociceptive information is modified before being relayed to higher centers, the second aim was to identify DH alterations that could modify the DH balance of excitation to inhibition. Specifically, we evaluated terminals of nociceptors and inhibitory neurons, potassium-chloride co-transporter 2 (KCC2) expression, and gliosis. A third aim was to develop a detection protocol for peripheral nerve growth factor (NGF) protein expression. Using histological approaches, we found that cartilage vascularization and other cartilage alterations were not detectable until a late time-point, at which time accompanying sympathetic and peptidergic fibers had invaded the cartilage. In the adjacent skin innervation changes included not only increased innervation of the upper-dermis and cartilage, as expected, but also an unexpected denervation of the epidermis. In the DH, we observed microgliosis, downregulation of a marker for inhibitory terminals and KCC2, suggesting disinhibition.

Methods

Animals

All experiments were performed in female and male Sprague Dawley (Charles River) rats (weighing 175g at arrival). Animals were housed 2 per cage with soft bedding on a 12-hour light/dark cycle with food and water available *ad libitum*. We followed the Care and Use of Experimental Animals of the Canadian Council on Animal Care guidelines and all studies were approved by the McGill University Faculty of Medicine Animal Care Committee. We followed the ARRIVE (Animal Research: Reporting of In Vivo Experiments) guidelines and checklist.

Arthritis model

Under 5% isoflurane in O₂ anesthesia, the right tibia-talus joint [7] was injected with 40μL that contained 40μg of CFA (Sigma) or mineral oil as a sham (shams). The total number of animals used in this study was 118, including those used for independent replications. Each finding was replicated a minimum of twice. Unless specified otherwise, each data set is 50% male data and 50% female data.

Ankle Width

Ankle swelling was assessed using a caliper to measure ankle width.

Behavioral Tests

Pain related behavior was assessed weekly from baseline to 4-weeks post-CFA using von Frey filaments to assess mechanical sensitivity, Hargreaves' test for heat hyperalgesia and acetone to assess cold allodynia. Beginning as close to 7 AM as possible, animals were habituated to the testing environment for 3 sessions before baseline measurements were recorded and at the beginning of each weekly session. Tests were applied in the same order as described below, with at least 15 minutes in between repeated tests, and 20 minutes from the last application of one test and the first application of the next to avoid sensitization from repeated testing. First, animals were habituated to the von Frey equipment until they had settled in a resting position. Filaments were applied according to the up-down method [16]; a sharp withdrawal was considered a positive response and the pattern of responses was used to calculate the 50% withdrawal threshold [10]. In the same testing equipment, the response in the 60 seconds following the application of an acetone drop was assessed as follows: 0 = no response, 1 = 1 sharp withdrawal, 2 = multiple lifts, 3 = sustained lifting, licking or vocalizations [11]. The average of 3 separate trials, with at least 5 minutes in between trials was calculated for each animal. Lastly, animals were habituated to the Hargreaves' testing apparatus [28] until they had settled in a resting position, with the hind paw resting flatly on the surface. The latency to a sharp withdrawal from a heat source was recorded from 3 separate trials (with at least 5 minutes in-between) and averages calculated for each animal. To avoid tissue damage, there was a stimulus-application limit of 20 seconds. All stimuli were applied to the plantar surface of the hind paw, adjacent to the ankle. Static weight distribution (SWD) was assessed with an Incapacitance Meter® (IITC Life Science 600/8) after animals walked on a treadmill (Columbus Instruments Exer 3/6), at 5.5m/min for 20 minutes. Three separate measurements over a 3-s period (averaged

automatically by the apparatus), were recorded for each rat after each walking session.

Measurements in grams were converted to the percentage of the total weight exerted by the hind paws that was distributed ipsilaterally [(ipsilateral weight/ipsilateral + contralateral weight) x 100]. In the week prior to baseline, animals were habituated to the treadmill and Incapacitance Meter® on 5 separate sessions.

Tissue Preparation

At 2- and 4-weeks post-CFA injection, under deep anesthesia with 0.3ml/100g of body weight of Equithesin (containing 12.75g of chloral hydrate, 3mg sodium pentobarbital and 6.38g of magnesium sulfate in solution, administered i.p.), animals were perfused through the left ventricle with perfusion buffer. For skin and joint extraction to be analyzed by immunohistochemistry this was followed by 3% paraformaldehyde (PFA) and 15% saturated picric acid in 0.1M phosphate buffer (pH 7.4) (PB). When only spinal cords were to be extracted, 4% PFA in PB was used (without picric acid). After fixation, hind-paw skin, ankle joints and lumbar spinal cords were extracted and post-fixed in the same fixative overnight (skin and spinal cords) or for 4 hours (joints) at 4°C. Joints were decalcified in 10% EDTA in dH₂O for 3 weeks and 3x rinsing in PB followed by phosphate buffered saline (PBS). Subsequently, skin and cords were cryoprotected in 30% sucrose in PBS and joints in 10% sucrose in 0.1M sodium cacodylate buffer overnight at 4°C. Tissue was embedded in optimum cutting temperature medium (OCT, Tissue Tek) and cut in a cryostat (Leica). Joints were cut at 25µm and attached to gelatin-subbed slides. Skin was cut at 50µm and spinal cords at 30µm, and sections were collected as free-floating in PBS. Glabrous hind-paw skin for analysis by western blot was extracted from another

cohort that was only perfused with perfusion buffer. We were able to collect synovial fluid from animals perfused with only buffer or fixative (by extracting it after perfusion buffer but before fixative). Briefly, a transverse incision was made across the dorsal ankle and the Achilles tendon punctured through until the joint capsule was also punctured. Using a pipette introduced through the puncture, synovial fluid was extracted by lavage (4x) with 25µl of 0.05M ethylenediaminetetraacetic acid (EDTA) (Sigma), pH7.5 [20], with a protease inhibitor (Roche). Samples were snap-frozen in liquid nitrogen and stored at -80°C for later processing.

Toluidine Blue Staining

After removing the OCT with dH₂O, ankle sections were stained with toluidine blue (0.04% toluidine blue in 0.2M acetic acid, pH 3.5) for 2 minutes. Sections were washed with dH₂O and dehydrated by one dip in 95% ethanol, 10 dips in 100% ethanol (x2), 2 minutes in xylene (x3). Slides were cover-slipped immediately with mounting medium (Entellan, EMD Millipore) and stored at room temperature. Mast cells and cartilage were identified by metachromatic staining and blood vessels by orthochromatic staining.

Immunohistochemistry

Skin and spinal cord immunohistochemistry (IHC) was carried out as previously described by us [37; 38]. Briefly, sections were washed 3 x with 0.2% Triton-X in PBS (PBST) to remove the OCT and blocked in 10% normal donkey or goat serum (NDS/NGS, species-matched to the secondary antibody) for 1 hour at room-temperature. Skin and joint sections were incubated in 50% ethanol for 30 minutes and washed 3 x with PBST before blocking. Primary antibody

incubations: anti-CD68 (mouse monoclonal, Bio-Rad, 1:500), anti-calcitonin gene related peptide (rabbit polyclonal, CGRP, Sigma, 1:2500), anti-vesicular GABA transporter (guinea pig polyclonal, VGAT, Synaptic Systems, 1:1000), anti-CD11b (mouse monoclonal, Bio-Rad, 1:100), anti-glia fibrillary acidic protein (mouse monoclonal, GFAP, Cell Signalling, 1:1000), anti-dopamine beta hydroxylase (mouse monoclonal, DBH, Medimabs, 1:50), anti-KCC2 (rabbit polyclonal, Millipore, 1:500), anti-PAX2 (R&D, 1:500) and Isolectin-IB4 conjugated to Alexa Fluor 488 (Invitrogen, 1:200), were carried out in 5% serum overnight at 4°C. The next day sections were washed 3 x with PBST and incubated with fluorochrome-conjugated secondary antibodies against the respective primary host (Invitrogen Alexa Fluor, Thermofisher) at 1:800 in PBST for 2 hours at room-temperature. Finally, sections were washed 3 x with PBST, mounted on gelatin subbed-slides and coverslipped with mounting medium (Vectashield, Vector). Microglia and macrophages were detected with anti-IBA1 (rabbit polyclonal, Wako, 019-19741) and anti-CD68 (mouse monoclonal, Biorad, MCA341Ga, 1:2000) antibodies with 3,3'-diaminobenzidine (DAB). For this, endogenous peroxidase was quenched with 0.3% H₂O₂ for 30 minutes, sections washed 3 x PBST and incubated in 5% NGS prior to overnight incubation with the primary antibodies at 4 °C. The next morning sections were washed 3 x with PBST and incubated for 1 hour at room temperature with a goat anti-mouse IgG (American Qualex, A106UU; diluted 1:50 in PBST), which had been pre-adsorbed with chopped, fixed rat lip tissue for 6hrs at 4 °C to prevent the known unspecific sticking of anti-mouse antibodies to connective tissue [48]. After 3 washes in PBST, sections were incubated with a mouse anti-HRP monoclonal antibody (1:30, Medimabs) pre-incubated with 5 µg/mL HRP. Following 3 washes in PBST, staining was developed with 0.06% DAB and 1% H₂O₂ in PBST. Sections were washed and mounted on gelatin-coated slides, dehydrated with a graded ethanol series, cleared in xylene and

cover-slipped with Entellan (EMD Millipore). For staining of microglia in the spinal cord the same protocol was used with the following differences; 1) 10% methanol + 3% H₂O₂ were used for quenching and 10% normal serum was used for blocking. 2) biotinylated goat anti-rabbit secondary (1:200 in PBST, Vector, BA-1000) was used, followed by the ABC complex from a Vectastain Elite ABC HRP kit (Vector). See the supplementary materials for details of IHC on joint tissue (available at <http://links.lww.com/PAIN/A967>).

Western blot

Following homogenization, samples were prepared for western blot with 1/3 loading buffer, 1/10 β-mercaptoethanol, sufficient sample and PBS to give appropriate final overall protein concentration. Tissue homogenization details can be found in the supplementary materials (available at <http://links.lww.com/PAIN/A967>). Whole skin lysate was prepared at 1 μg/μl for the detection of proNGF and concentrated softly homogenized skin at 1.2 μg/μl. For synovial fluid, samples were prepared with the above proportions of loading buffer and β-mercaptoethanol and the remainder the concentrated extract. After boiling for 5 minutes, 15 μl of samples were resolved on a 15% gel at 90mV, therefore, approximately 10 μl of concentrated synovial extracts were resolved. Subsequently proteins were transferred to a PVDF membrane (Bio-Rad) at 30mA for 90 minutes. Due to different blocking (and later exposure time) requirements for the detection of proNGF and mature NGF (mNGF), membranes were cut at ~20kDa indicated by a molecular weight standard (Biorad). This was then blocked for 1 hour at room temperature with 5% milk for higher molecular weights and 2.5% bovine serum albumin (BSA) for lower molecular weights prior to overnight incubation at 4°C in primary antibodies against NGF. Rabbit anti-proNGF (Alomone, AN005, 1:200) was diluted in 5% milk and rabbit

anti-NGF (Abcam, ab979, 1:500) in 1% BSA. Secondary antibody incubations (donkey anti-rabbit conjugated to HRP, Jackson 711036152, 1:10000) were carried out at room temperature following which the signal was revealed with ECL and developer (Kodak). NGF levels from whole skin lysate were normalized to β -actin. Since the softly homogenized skin protocol was designed to enrich for extracellular protein levels, total protein content was assessed with Ponceau S staining and used as loading control. As no protein was detectable in contralateral synovial fluid, samples were prepared with equal extract volume instead of equal protein concentration and there was no appropriate loading control. Densitometric analyses were carried out using a flat-bed scanner and ImageJ.

Imaging

Microscopy was carried out using a Zeiss AxioImager M2 Imaging microscope. For bright field imaging, we used a Zeiss AxioCam 506 Color for real-color image capturing; for fluorescence images, an AxioCam 512 Monochrome camera with pseudo-color was used. Exceptionally, VGAT and KCC2 signals were captured with a Zeiss LSM800 confocal microscope. Both microscopes were used with the Zeiss ZenPro software v.2.3 (Zeiss Canada). For each staining, acquisition settings were kept consistent for all images taken.

Vascularization Quantification

We analyzed 3 joint sections from each animal for all cartilage alterations assessed; individual images were taken with a 10x objective and stitched in the microscope software to form 1 large tiled image per section covering the articular cartilages of the talus and tibia and adjacent tissues.

We used the ImageJ freehand line tracer to measure the length of the cartilage of both bones. We defined a cartilage vascularization point as a blood vessel clearly penetrating the tide-mark that separates the calcified from non-calcified cartilage at the osteochondral junction. The number of vascularization points per millimeter was calculated for each bone, for each section.

Cartilage thickness

Using the ImageJ freehand line tracer, 3 measurements of cartilage thickness were taken from both bones (a total of 6 measurements per joint) for the 3 sections per animal. Measurements were taken from the cartilage edges (and an average calculated) and one measurement from the middle of the cartilage.

Cartilage Damage Scoring

Damage was assessed with a cartilage erosion grading scale [8] from 0 to 4. A score of 0 would demonstrate no erosion, 1 would indicate a small amount of erosion located to one area, 2 would express moderate erosion in a limited number of areas, 3 would signify erosion in several areas. Finally, a score of 4 would indicate general erosion.

Optical Density in Cartilage

In ImageJ, the images were converted into 8-bit; regions of interest were selected, optical density measured, and values subtracted from 255 (255=white, 0=black in 8-bit images) for a higher value to represent darker staining. For each section, 3 measurements were taken from each bone,

for a total of 6 values per section. The same process was used to analyze the optical density of western blot bands.

Fiber Density

Sympathetic fiber innervation of the skin was quantified as previously described [37].

Sympathetic fibers in the joint, and peptidergic fibers in both skin and joint were quantified with the ImageJ freehand line tracer and expressed as length per unit area. As in previous publications from our laboratory, we define the upper dermis as the region within 150 μ m from the dermal-epidermal junction [61].

Spinal Cord Image Analyses

Central terminals of nociceptors (labelled with IB4 and CGRP), CD68, KCC2 and VGAT signals were quantified by the average intensity of staining in ImageJ in images captured using a 10x objective for IB4 and CGRP, a 20x objective for CD68 and KCC2, and a 63x oil immersion lens for VGAT. The CR3 signal was quantified by the area occupied by the staining on images captured with a 20x objective. To analyze glial cells, stacked images gathered with a 40x objective (spanning 30 μ m depth with a z-step of 1 μ m) were processed using the “Extended Depth of Processing” feature in Zeiss software. The subsequent image generated was used for a manual count of astrocyte and microglial cell bodies. Morphological analysis was carried out as previously described [27; 34]. In total, 3-6 images taken from the medial 2/3 of the dorsal horn were analyzed per animal. To analyze KCC2, 6 ROIs from lamina I and lamina II were selected.

Experimental design and statistical analyses

Samples sizes were selected based on previous studies from our lab (including preliminary studies of the work presented here), discussions with field experts, and standard practices in the preclinical pain field [33]. We conducted *post-hoc* power analyses of data from previous studies to confirm appropriateness. Means were calculated from the 3 sections per animal and subsequently used to calculate group means. All statistical tests were completed using Windows GraphPad Prism version 5. Behavioral and cartilage alteration data were assessed with two-way ANOVAs, innervation and spinal cord data were analyzed by student's t-tests and paired t-tests when pairs of ipsilateral and contralateral data were being analyzed. Preliminary studies showed that there was no difference between contralateral and sham measurements, and therefore the contralateral tissue was used as a control for analyses, except microglial morphology analyses in which shams served as controls as preliminary studies revealed that contralateral IBA1 staining was not the same as in shams.

Results

CFA-induced lasting hypersensitivities and ankle swelling

No sex differences were observed in any of the parameters assessed in the study, hence we have pooled male and female animals together. For succinctness and clarity, we have only included the pooled data.

Behavioral assessment of the contralateral paw was carried out concurrently; because no notable effects were observed from baseline, these data have been omitted for clarity. The injection of CFA into the ankle joint induced mechanical and cold hypersensitivities, together with ankle-swelling, for the duration of the experiment (Figure 1; two-way repeated measures ANOVA; von Frey - $F < 0.0001$ for time factor, paw factor and interaction $F(1.871, 35.55) = 614.6$, $P < 0.0001$ [time factor], $F(1.000, 19.00) = 7922$, $P < 0.0001$ [paw factor], $F(1.871, 35.55) = 614.6$, $P < 0.0001$ [interaction]; acetone - $F(4, 76) = 44.99$, $P < 0.0001$ [time factor], $F(1, 19) = 154.6$, $P < 0.0001$ [paw factor], $F(4, 76) = 44.27$, $P < 0.0001$ [interaction]; Ankle swelling - $F(1, 11) = 0.09813$, $P = 0.7599$ [time factor], $F(1, 11) = 162.0$, $P < 0.0001$ [paw factor], $F(1, 11) = 0.2189$, $P = 0.6490$ [interaction]. Cold sensitivity was absent at baseline and for contralateral values, with increased pain behaviors lifting, shaking and licking of the paw in 60 seconds observed at all post-CFA time-points assessed (Figure 1A). Decreased 50% withdrawal threshold to von Frey fiber application demonstrated the presence of mechanical sensitivity. At baseline and for contralateral assessments the upper cut-off was almost always reached and were therefore assigned a value of 24g. Mean ipsilateral values dropped to a low of a 2.4g (Figure 1B) from 1-week post-CFA onwards. The Hargreaves' test of heat hyperalgesia could not be applied at 1- or 2-weeks post-CFA due to guarding of the inflamed paw, which recovered by week 3. At that time only, heat hyperalgesia was transiently present as decreased withdrawal latency of the ipsilateral paw (Figure 1C; two-way repeated measures ANOVA; $F(2, 38) = 4.784$, $P = 0.0140$ [time factor], $F(1, 19) = 6.767$, $P = 0.0175$ [paw factor], $F(2, 38) = 3.936$, $P = 0.0280$ [interaction]). At earlier time-points, we observed paw guarding and swelling of the ipsilateral paw that extended beyond the ankle. These were observed to accompany one another, and both resolved by 3 weeks. To assess pain-related to movement weight bearing across the hind paws

was measured after animals had walked for 20 minutes on a treadmill. Static weight distribution (SWD) was reduced from baseline and from contralateral measurements from 1-week post-CFA onwards, recovering from peak levels but lasting through to 4 weeks post-CFA (Figure 1E; two-way repeated measures ANOVA; $F(4, 20) = 1.000$, $P=0.4307$ [time factor], $F(1, 5) = 159.0$, $P<0.0001$ [paw factor], $F(4, 20) = 17.39$, $P<0.0001$ [interaction]). Taken together, these data suggest that CFA induces lasting inflammation of the joint and persistent hypersensitivity.

CFA-induced cartilage alterations

A primary objective of this study was to provide a time course illustrating that pathological joint changes do not become apparent in this model of IA until relatively late post-CFA. As a previous study from our lab has identified a divergence of mechanisms contributing to pain in this model at 2- and 4-weeks post-CFA [37], these were the time points examined here. Despite the early emergence and persistence of pain-related behavior, the cartilage alterations that we assessed were not detectable until 4-weeks post-CFA. At the later time-point, vascularization of the ipsilateral talus and tibial cartilage was detectable as sites where blood vessels clearly penetrated the tidemark (Figure 2A, B; two-way ANOVA; $F(1, 56) = 114.2$, $P<0.0001$ [time factor], $F(3, 56) = 30.14$, $P<0.0001$ [paw factor], $F(3, 56) = 30.10$, $P<0.0001$ [interaction]). Vascularization of the ipsilateral tibia was found to be statistically significantly lower than that of the talus at 4 weeks post-CFA (Figure 2A, B; $p = 0.0026$ by Bonferroni corrected post-hoc t-test).

The thickness of the darkly stained cartilage had thinned from contralateral measurements at the midpoint of the ipsilateral talus at 4-weeks post-CFA (Figure 2A, C; two-way ANOVA; $F(1, 27) = 0.5025$, $P=0.4845$ [time factor], $F(1, 27) = 5.234$, $P=0.0302$ [paw factor], $F(1, 27) = 0.7180$,

$P=0.4043$ [interaction]). This was the sole mean cartilage thickness measurement that was found to be different between ipsilateral and contralateral measurements (data from other measurements not shown). At the same time, toluidine blue staining of the cartilage of both ipsilateral ankle bones was found to be 33% less dark than contralateral measurements (Figure 2A, D; two-way ANOVA; $F(1, 28) = 19.01$, $P=0.0002$ [time factor], $F(1, 28) = 13.92$, $P=0.0009$ [paw factor], $F(1, 28) = 17.92$, $P=0.0002$ [interaction]), which suggests a decrease in proteoglycan content. Finally, using a damage score [8], damage was only present in ipsilateral joints at 4-weeks post-CFA (Figure 2E; two-way ANOVA; $F(1, 28) = 47.48$, $P<0.0001$ [time factor], $F(1, 28) = 137.8$, $P<0.0001$ [paw factor], $F(1, 28) = 31.09$, $P<0.0001$ [interaction]). Although the talus damage score did not reach the peak possible measurement even at four weeks post-CFA, there was generalized and widespread destruction to the talus. The situation was not the same in the tibia, where more localized destruction was observed. At both timepoints, the hypertrophic pannus was clearly present and at 4 weeks the pannus could be seen invading the cartilage from the joint space.

Altered peripheral innervation and upregulated NGF in CFA-induced arthritis

In previous studies altered peripheral innervation in this model has been demonstrated at 4 weeks post-CFA only. For this reason, plus the late emergence of cartilage alterations, the later timepoint was the focus of experiments investigating nervous system alterations. As previously reported [37], sympathetic innervation of the upper dermis was increased at 4 weeks post-CFA in ipsilateral skin (Figure 3A, B; $t(8) = 2.695$, $p = 0.0273$ by paired t-test). Ipsilateral upper dermal innervation by peptidergic fibers was also increased (Figure 3A,B; $t(7) = 2.564$, $p = 0.0373$ by

paired t-test), but interestingly, epidermal innervation by the same fibers was decreased (Figure 3A, B; $t(9) = 2.819$, $p = 0.0201$ by paired t-test). In both the skin and synovium, peptidergic fibers and sympathetic fibers were observed wrapping around one another (Figure 4A, C).

Unexpectedly, a transient dermal and hypodermal inflammatory infiltration was observed (Figure 4 A-D). At 2-weeks post-CFA there was a significant increase in the number of mast cells in the upper dermis of the ipsilateral paw compared to the contralateral side (Figure 4A-B, $F(1,13) = 21.31$, $p = 0.0005$ by two-way ANOVA with post hoc t-test) which by 4-weeks post-CFA was no longer detectable. In parallel, there was a large inflammatory infiltration of the lower dermis and hypodermis (containing mast cells, macrophages, and other mononuclear cells) of the ipsilateral paw at 2 weeks only (Figure 4C). Unsurprisingly, cell infiltration of the synovium persisted until 4 weeks (Figure 4E).

Innervation changes in the joint were similar to those observed in the skin. Abnormal cartilage innervation by sympathetic and peptidergic fibers was detectable in the ipsilateral joint at 4 weeks (Figure 5). As we had observed greater alterations to the talus (Figure 2), and previously we could detect sprouting at 4-weeks post-CFA only [37], cartilage innervation was assessed in this bone at this time point only. Sprouted sympathetic and peptidergic fibers in the cartilage were observed associated with blood vessels as small, fine fibers, with small varicosities (Figure 5A, B, C; VMAT2: $t(3) = 6.676$, $p = 0.0069$, CGRP: $t(3) = 6.837$, $p = 0.0064$ by paired t-test). This morphology is consistent with newly sprouted fibers. Although we did not quantitate synovial innervation or inflammatory cell infiltration, we observed at 4 weeks increased innervation in CFA-treated animals and, like in the skin, a novel arrangement of sympathetic and peptidergic varicosities in close apposition, which did not occur in controls (Figure 3C). In

keeping with the nature of the pannus, a large inflammatory infiltration was observed in synovial tissue (not shown).

The detection of NGF was in itself a challenge. Homogenization of whole skin gave a lysate that was unsuitable for mNGF analysis by western blot with the available antibodies. Using an altered, more gentle homogenization protocol combined with concentrating sample proteins by precipitation with methanol and chloroform, we were able to detect upregulated mNGF in ipsilateral synovial fluid and adjacent glabrous skin (Figure 6; synovial fluid: $W(0,45) = 45$, $p = 0.0039$, skin: $W(28, 0) = 28$, $p = 0.0156$ by Wilcoxon signed rank). This band is of the expected molecular weight of 13.5kDa and aligned with that corresponding to recombinant human NGF. In skin samples, in addition to the 13.5kDa band that aligns with the positive control and the band in ipsilateral synovial fluid, we observed another band of slightly lower molecular weight. It is difficult to tell if this represents another isoform of NGF or a spurious band resulting from the problematic nature of probing low abundance proteins from a biological sample such as skin. Detection of proNGF did not have the same initial issues as mNGF and could be detected using a much lower overall protein concentration than was needed for the mature form. Interestingly, proNGF was detected at different molecular weights, which changed differentially depending on tissue and homogenization method. A band migrating at around 25kDa, a characterized molecular weight [50] that migrated alongside recombinant proNGF, was upregulated in whole skin lysate (Figure 6 B; $U = 0.0$, $p = 0.0286$ by Mann Whitney). This band was absent from synovial fluid and gently homogenized skin; these samples contained proNGF migrating at 40kDa which is upregulated in ipsilateral synovial fluid (Figure 6; synovial fluid: $W(0,45)=45$, $p = 0.0035$, skin: $W(19, -9) = 10$, $p = 0.4688$ by Wilcoxon signed rank). The 40kDa form was present at the same concentration in CFA-treated and control whole skin lysate (Figure 6 B; W

(9, -1) = 8, $p=0.25$ by Wilcoxon signed rank). This agrees with previous findings [37], and has been reported as a glycosylated form of proNGF [49]. Upregulated NGF was detectable from timepoints sampled across the duration of the experiment, but for clarity only samples from 4 weeks post-CFA are shown. Synovial fluid extracted from the ipsilateral ankle contained more overall protein than fluid taken from the contralateral (data not shown).

CNS alterations

Given the alterations to peptidergic nociceptors in the periphery, we wondered if there were changes to their DH terminals. However, we did not detect any difference between ipsilateral and contralateral DH measurements of the average intensity of the fluorescent signals of CGRP or IB4 (Figure 7; CGRP: $t(8) = 0.3847$, $p = 0.7105$, IB4: $t(8) = 0.07797$, $p=0.9398$ by paired t-test). We did not observe an ipsilateral-contralateral difference in the number of astrocytes as detected by GFAP staining, or in area occupied by them (Figure 8A-B; number: $t(9) = 0.915$, $p=0.3840$, area: $t(7) = 2.186$, $p = 0.0650$ by paired t-test), suggesting a lack of astrogliosis.

Microgliosis on the other hand, was observed at 4-weeks post-CFA as increased microglial cell density and altered morphology (decrease of the length/area ratio of cells) in ipsilateral DH compared to shams (Figure 8C-D; density: $t(16) = 6.842$, $p<0.0001$, morphology: $t(13) = 2.758$, $p = 0.0163$ by student's t-test). Unlike our previous findings at 2 weeks in this model where peripheral nerves sprouting was not detectable [37], at 2 weeks post-CFA microgliosis was already detectable (Figure 8C-D). We did not detect any differences between the number of microglia or their morphology comparing contralateral to sham, but by visual examination it can be seen that in the contralateral DH microglia do not appear exactly the same as in sham (Figure 8D). Microglial activation markers CR3 and CD68 (Figure 9 A, B, C) were upregulated in the

ipsilateral DH with increased area occupied by CR3 staining (Figure 9 A, C; $t(9) = 3.814$, $p = 0.0041$ by student's t-test), and increased mean intensity of the CD68 signal (Figure 9 B, C; $U = 3$, $p = 0.0341$ by Mann Whitney). Together, these data suggest that microglia infiltrate the area of the spinal cord where primary afferents innervating the ankle joint terminate, and that these cells have an altered function from normal. Finally, at 4 weeks post-CFA ipsilateral DH immunoreactivity intensity for VGAT, an inhibitory terminal marker, and potassium chloride transporter KCC2 were reduced compared to control (Figure 9 D-E; VGAT: $t(16) = 2.16$, $p = 0.0463$, KCC2: $t(4) = 7.295$, $p = 0.0019$ by students t-tests).

Discussion

This study demonstrates that pathology in IA extends beyond joint inflammation, encompassing decreased joint integrity, peripheral innervation changes, and DH alterations that could alter the balance of inhibition to excitation. In the DH, there was evidence of microgliosis, KCC2 downregulation and selective inhibitory terminal loss. While addressing the main aims of this work, we provided evidence that many arthritis-related joint changes do not occur until later stages even though pain related behaviour emerges early.

The cartilage alterations described in this manuscript are the first rigorous, quantitative analysis of cartilage changes following CFA treatment. As mechanisms underlying pain in early and late stage disease likely differ, selection of appropriate endpoints in preclinical studies is necessary. Given that this is contingent on knowing when changes occur, the quantitative time-course provided here fills a notable literature gap by providing measurable outcomes that can guide the design of future interventional experiments. The observed reduction in cartilage integrity,

thinning, proteoglycan loss and altered structure, would render the cartilage less effective in conducting its roles of protecting the underlying bone and maintaining phenotypic stability of chondrocytes. In this altered environment, chondrocytes may contribute directly to the inflammatory and pronociceptive milieu of the inflamed joint [32].

The innervation data raise multiple discussion points and serve three important purposes: the confirmation in females of previously demonstrated fibre sprouting, demonstration of fibre sprouting in the cartilage, and the description of complex innervation changes in the skin. In previous investigations [37], examination of sprouting in the joint following CFA treatment was restricted to the synovial membrane in male rodents. Here we show that blood vessels accompanied by sympathetic and peptidergic fibres invade the cartilage, in males and females. The observed *de novo* innervation of the cartilage brings nociceptors into close proximity with both the altered cartilage matrix and synovial fluid that contains inflammatory and pronociceptive mediators (such as NGF, as detected here). The observed vascular invasion of the cartilage is thus a double-whammy, by bringing nociceptors into an altered and now pronociceptive environment. Although these findings suggest that a sympathetic nervous system participation in pain in the late stage of this model [37] may also apply to females, it will be important to elucidate if sympathectomy attenuates pain in females. Lastly, the observed skin innervation changes involve parallel hyperinnervation of one anatomical region and denervation of another. Potentially indicative of complex rearrangement processes involving both retraction and sprouting mechanisms, this highlights how complex nervous system alterations could be in chronic joint pain.

Interestingly, we observed transient infiltration of mast cells into the same region of the skin in which fibers sprouted. Mast cells release NGF [35] and, as they express trkA, peptidergic and sympathetic fibers respond to NGF [24; 36]. Therefore, NGF-releasing cell infiltration preceding NGF-responsive cell sprouting into the same zone may point to a driving-process. In addition to being the likely driver of peptidergic and sympathetic sprouting, NGF is an effective mediator of primary afferent sensitization [9]. As such, NGF is already identified as a potential multi-modal target for the treatment of arthritis pain, however, currently, the anti-NGF antibodies that demonstrated great pain-relief effects await FDA approval after side-effects emerged in trials [5].

In the CNS, extra-cellular proNGF cleavage has been shown [6], contrasting with earlier studies assuming that, like mouse submandibular gland derived NGF, all NGF was cleaved intracellularly [18]. To our knowledge, the peripheral release and processing pathway of NGF has not been clarified. In part this is because detection of mNGF has been rather difficult, especially in peripheral tissues, which is why this work includes a description of the detection method. The detection of different molecular weights across tissue-type and the upregulation of different molecular weights in ipsilateral samples point to intriguing potential processing differences between the different molecular weights of proNGF. Indeed, proNGF is not the biologically inactive precursor of mNGF, but is itself biologically active [17], and the ratio of precursor to mature is important for a normal neuronal state [14]. Elucidation of peripheral release and conversion of NGF, especially in painful conditions, will be vital for optimal refinement of anti-NGF based treatments to maximize the superior pain-relief whilst reducing side-effects.

The second aim was to identify DH alterations that could alter the balance of excitation to inhibition. There is no doubt that from an inflamed joint there will be increased transduction from primary afferents to the DH and it is well established that peripheral and central sensitization occur in arthritis [42]. Hyperexcitability of nociceptive projection neurons in joint pain models has been demonstrated [25], but it is not known if this is driven by only increased peripheral drive and central excitatory changes [2; 40; 45; 46; 52] or if there is also a contribution from decreased inhibition. Upregulation of substance P and CGRP have been shown in the DH in IA models [19; 40; 51], as well as changes of the substance P receptor expression [2; 51]. The discrepancy in CGRP immunoreactivity in the spinal cord between studies [19], including ours, may be due to differences in signal quantification method, idiosyncrasies between models or the time-points of sampling. Specifically, in the current model there was visibly less tissue inflammation due to the lower dose of CFA than in previous models used by us [37; 51].

Here, we show for the first time that in the IA-CFA model inhibitory neural connections appear to be lost and KCC2 is downregulated. As both of these are important for the maintenance of normal DH inhibition in pain processing, this opens the door to the hypothesis that DH disinhibition occurs in arthritis. Moreover, to our knowledge, this is the first analysis of microglial morphology in the dorsal horn in CFA-treated animals. The altered microglial function inferred here by the morphological changes deserves further attention, including contralateral side alterations. Although beyond the scope of this study, it is noteworthy that a difference was observed visually. This could be due to systemic inflammation, or represent subtle CNS changes that could be related to widespread sensitivity often present in IA patients even when inflammation is controlled [4]. Microglia have been implicated in arthritis, [3; 12; 19]

but as a role for microglia has been demonstrated in DH disinhibition associated with a different chronic pain condition, neuropathic pain [15], we believe that this may also be relevant in arthritis. Characteristics associated with neuropathic pain such as burning, pain from light pressure and spontaneous shock-like pain are also reported by IA patients when describing their pain. These reports are not infrequent (up to 36% of patients) [47] and preclinical studies have noted similarities between neuropathic and arthritis animal models [55]. The combined presence of microgliosis and changes that point towards DH disinhibition strengthen the perspective that arthritis and neuropathic pain may share features and underlying mechanisms. The details of this potential indication of the presence of disinhibition in arthritis warrant further investigation and may point to the use of drugs that act centrally to treat pain in arthritis. Indeed, interest in the use of gabapentinoids and duloxetine (first-line neuropathic pain agents that act on calcium channels and the noradrenergic-serotonergic system, respectively) is increasing [53]. Although we draw parallels with mechanisms in neuropathic and arthritis pain, it cannot yet be determined if these represent a “neuropathic component” to arthritis pain or if these are commonalities between these two, and potentially more, chronic pain conditions.

Limitations of this study include that the changes described here are currently only associated with pain and other types of studies will be necessary (for example genetic or pharmacological approaches) to demonstrate a causative link to pain. This is particularly relevant regarding the functional role of sprouted sympathetic fibers in females, as previously histological changes in pain models have been shown to occur in both sexes, but functional, downstream sexual dimorphisms have been identified in the spinal cord [54]. The implications of the decreased VGAT and KCC2 signals are intriguing, but the consequences and cause of these remain undetermined. Our lab is currently carrying out a more comprehensive analysis of inhibitory and

excitatory synapses in the DH of arthritis and neuropathic pain models. Although this study presents an anatomical basis for nervous system changes on both sides of the balance in DH excitability, comprehensive physiological functional studies will be needed to understand how these findings contribute to pain in IA.

With these extensive analyses, we hope to reiterate the importance of regarding pain in arthritis in an integrated way, by which the identification of novel mechanistic targets may arise. Together, the complex findings in the periphery and CNS presented here suggest that in arthritis there may be a shift in the balance between incoming and outgoing excitation, and modulatory inhibitory tone in the DH.

Acknowledgements

This work was supported by CIHR operating grant MOP-136903 to ARS. SL, NY and VB acknowledge studentships from the Louise and Alan Edwards Foundation. We acknowledge Min-Ju Lee for help in data gathering, Jean-Francois Trempe, McGill University for his help with protein precipitation and Camilla Svensson, Karolinska Institute for assistance with synovial fluid extraction and NGF antibody protocol advice.

References

- [1] Almarestani L, Longo G, Ribeiro-da-Silva A. Autonomic fiber sprouting in the skin in chronic inflammation. *Molecular pain* 2008;4:56.
- [2] Almarestani L, Waters SM, Krause JE, Bennett GJ, Ribeiro-da-Silva A. De novo expression of the neurokinin 1 receptor in spinal lamina I pyramidal neurons in polyarthritis. *The Journal of comparative neurology* 2009;514(3):284-295.
- [3] Bas DB, Su J, Sandor K, Agalave NM, Lundberg J, Codeluppi S, Baharpoor A, Nandakumar KS, Holmdahl R, Svensson CI. Collagen antibody-induced arthritis evokes persistent pain with spinal glial involvement and transient prostaglandin dependency. *2012;64(12):3886-3896.*
- [4] Basu N, Kaplan CM, Ichesco E, Larkin T, Harris RE, Murray A, Waiter G, Clauw DJ. Neurobiologic Features of Fibromyalgia Are Also Present Among Rheumatoid Arthritis Patients. *Arthritis & Rheumatology* 2018;70(7):1000-1007.
- [5] Brown MT, Murphy FT, Radin DM, Davignon I, Smith MD, West CR. Tanezumab reduces osteoarthritic hip pain: results of a randomized, double-blind, placebo-controlled phase III trial. *Arthritis and rheumatism* 2013;65(7):1795-1803.
- [6] Bruno MA, Cuello AC. Activity-dependent release of precursor nerve growth factor, conversion to mature nerve growth factor, and its degradation by a protease cascade. *Proceedings of the National Academy of Sciences of the United States of America* 2006;103(17):6735-6740.
- [7] Butler SH, Godefroy F, Besson JM, Weil-Fugazza J. A limited arthritic model for chronic pain studies in the rat. *Pain* 1992;48(1):73-81.

- [8] Camps M, Ruckle T, Ji H, Ardisson V, Rintelen F, Shaw J, Ferrandi C, Chabert C, Gillieron C, Francon B, Martin T, Gretener D, Perrin D, Leroy D, Vitte PA, Hirsch E, Wymann MP, Cirillo R, Schwarz MK, Rommel C. Blockade of PI3Kgamma suppresses joint inflammation and damage in mouse models of rheumatoid arthritis. *Nat Med* 2005;11(9):936-943.
- [9] Chang DS, Hsu E, Hottinger DG, Cohen SP. Anti-nerve growth factor in pain management: current evidence. *Journal of Pain Research* 2016;9:373-383.
- [10] Chaplan SR, Bach FW, Pogrel JW, Chung JM, Yaksh TL. Quantitative assessment of tactile allodynia in the rat paw. *J Neurosci Methods* 1994;53(1):55-63.
- [11] Choi Y, Yoon YW, Na HS, Kim SH, Chung JM. Behavioral signs of ongoing pain and cold allodynia in a rat model of neuropathic pain. *Pain* 1994;59(3):369-376.
- [12] Clark AK, Grist J, Al-Kashi A, Perretti M, Malcangio M. Spinal cathepsin S and fractalkine contribute to chronic pain in the collagen-induced arthritis model. 2012;64(6):2038-2047.
- [13] Coggeshall RE, Hong KA, Langford LA, Schaible HG, Schmidt RF. Discharge characteristics of fine medial articular afferents at rest and during passive movements of inflamed knee joints. *Brain research* 1983;272(1):185-188.
- [14] Costa RO, Perestrelo T, Almeida RD. PRoneurotrophins and CONsequences. *Molecular neurobiology* 2018;55(4):2934-2951.
- [15] Coull JA, Beggs S, Boudreau D, Boivin D, Tsuda M, Inoue K, Gravel C, Salter MW, De Koninck Y. BDNF from microglia causes the shift in neuronal anion gradient underlying neuropathic pain. *Nature* 2005;438(7070):1017-1021.

- [16] Dixon WJ. Efficient analysis of experimental observations. *Annual review of pharmacology and toxicology* 1980;20:441-462.
- [17] Fahnestock M, Shekari A. ProNGF and Neurodegeneration in Alzheimer's Disease. *Frontiers in Neuroscience* 2019;13(129).
- [18] Fahnestock M, Yu G, Coughlin MD. ProNGF: a neurotrophic or an apoptotic molecule? *Progress in brain research* 2004;146:101-110.
- [19] Fernandez-Zafra T, Gao T, Jurczak A, Sandor K, Hore Z, Agalave NM, Su J, Estelius J, Lampa J, Hokfelt T, Wiesenfeld-Hallin Z, Xu X, Denk F, Svensson CI. Exploring the transcriptome of resident spinal microglia after collagen antibody-induced arthritis. *2019;160(1):224-236.*
- [20] Finn A, Angeby Moller K, Gustafsson C, Abdelmoaty S, Nordahl G, Ferm M, Svensson C. Influence of model and matrix on cytokine profile in rat and human. *Rheumatology (Oxford)* 2014;53(12):2297-2305.
- [21] Flodin P, Martinsen S, Altawil R, Waldheim E, Lampa J, Kosek E, Fransson P. Intrinsic Brain Connectivity in Chronic Pain: A Resting-State fMRI Study in Patients with Rheumatoid Arthritis. *Frontiers in human neuroscience* 2016;10:107.
- [22] Ghilardi JR, Freeman KT, Jimenez-Andrade JM, Coughlin KA, Kaczmarek MJ, Castaneda-Corral G, Bloom AP, Kuskowski MA, Mantyh PW. Neuroplasticity of sensory and sympathetic nerve fibers in a mouse model of a painful arthritic joint. *Arthritis and rheumatism* 2012;64(7):2223-2232.
- [23] Gladman DD, Thavaneswaran A, Chandran V, Cook RJ. Do patients with psoriatic arthritis who present early fare better than those presenting later in the disease? *Annals of the Rheumatic Diseases* 2011;70(12):2152-2154.

- [24] Gorin PD, Johnson EMJ. Effects of long term nerve growth factor deprivation on the nervous system of rat: an experimental autoimmune approach. *Brain research* 1980;198:27-42.
- [25] Grubb BD, Stiller RU, Schaible HG. Dynamic changes in the receptive field properties of spinal cord neurons with ankle input in rats with chronic unilateral inflammation in the ankle region. *Experimental brain research* 1993;92(3):441-452.
- [26] Guilbaud G, Iggo A, Tegner R. Sensory receptors in ankle joint capsules of normal and arthritic rats. *Experimental brain research* 1985;58(1):29-40.
- [27] Hanzel CE, Pichet-Binette A, Pimentel LS, Iulita MF, Allard S, Ducatenzeiler A, Do Carmo S, Cuello AC. Neuronal driven pre-plaque inflammation in a transgenic rat model of Alzheimer's disease. *Neurobiology of aging* 2014;35(10):2249-2262.
- [28] Hargreaves K, Dubner R, Brown F, Flores C, Joris J. A new and sensitive method for measuring thermal nociception in cutaneous hyperalgesia. *Pain* 1988;32(1):77-88.
- [29] Hashmi JA, Yashpal K, Holdsworth DW, Henry JLJR. Sensory and vascular changes in a rat monoarthritis model: prophylactic and therapeutic effects of meloxicam. 2010;59(8):667-678.
- [30] Haywood AR, Hathway GJ, Chapman V. Differential contributions of peripheral and central mechanisms to pain in a rodent model of osteoarthritis. *Scientific reports* 2018;8(1):7122.
- [31] He BH, Christin M, Mouchbahani-Constance S, Davidova A, Sharif-Naeini R. Mechanosensitive ion channels in articular nociceptors drive mechanical allodynia in osteoarthritis. *Osteoarthritis and cartilage* 2017;25(12):2091-2099.

- [32] Kapoor M, Martel-Pelletier J, Lajeunesse D, Pelletier J-P, Fahmi H. Role of proinflammatory cytokines in the pathophysiology of osteoarthritis. *Nature Reviews Rheumatology* 2010;7:33.
- [33] Kimmelman J, Mogil JS, Dirnagl U. Distinguishing between Exploratory and Confirmatory Preclinical Research Will Improve Translation. *PLOS Biology* 2014;12(5):e1001863.
- [34] Lee TT, Skafidas E, Dottori M, Zantomio D, Pantelis C, Everall I, Chana G. No preliminary evidence of differences in astrocyte density within the white matter of the dorsolateral prefrontal cortex in autism. *Mol Autism* 2017;8:64.
- [35] Leon A, Buriani A, Dal Toso R, Fabris M, Romanello S, Aloe L, Levi-Montalcini R. Mast cells synthesize, store, and release nerve growth factor. *Proceedings of the National Academy of Sciences of the United States of America* 1994;91(9):3739-3743.
- [36] Lewin GR, Barde YA. Physiology of the neurotrophins. *Annual review of neuroscience* 1996;19:289-317.
- [37] Longo G, Osikowicz M, Ribeiro-da-Silva A. Sympathetic fiber sprouting in inflamed joints and adjacent skin contributes to pain-related behavior in arthritis. *The Journal of neuroscience : the official journal of the Society for Neuroscience* 2013;33(24):10066-10074.
- [38] Lorenzo LE, Magnussen C, Bailey AL, St Louis M, De Koninck Y, Ribeiro-da-Silva A. Spatial and temporal pattern of changes in the number of GAD65-immunoreactive inhibitory terminals in the rat superficial dorsal horn following peripheral nerve injury. *Molecular pain* 2014;10:57.
- [39] Ma QP, Woolf CJ. Basal and touch-evoked fos-like immunoreactivity during experimental inflammation in the rat. *Pain* 1996;67(2-3):307-316.

- [40] Malcangio M, Bowery NG. Calcitonin gene-related peptide content, basal outflow and electrically-evoked release from monoarthritic rat spinal cord in vitro. *Pain* 1996;66.
- [41] McWilliams DF, Dawson O, Young A, Kiely PD, Ferguson E, Walsh DA. Discrete trajectories of resolving and persistent pain in people with rheumatoid arthritis despite undergoing treatment for inflammation: Results from three UK cohorts. *The journal of pain : official journal of the American Pain Society* 2019.
- [42] McWilliams DF, Walsh DA. Pain mechanisms in rheumatoid arthritis. *Clinical and experimental rheumatology* 2017;35 Suppl 107(5):94-101.
- [43] Meeus M, Vervisch S, De Clerck LS, Moorkens G, Hans G, Nijs J. Central sensitization in patients with rheumatoid arthritis: a systematic literature review. *Seminars in arthritis and rheumatism* 2012;41(4):556-567.
- [44] Miller RE, Ishihara S, Bhattacharyya B, Delaney A, Menichella DM, Miller RJ, Malfait AM. Chemogenetic Inhibition of Pain Neurons in a Mouse Model of Osteoarthritis. *Arthritis & rheumatology (Hoboken, NJ)* 2017;69(7):1429-1439.
- [45] Nieto FR, Clark AK, Grist J, Chapman V, Malcangio M. Calcitonin Gene-Related Peptide-Expressing Sensory Neurons and Spinal Microglial Reactivity Contribute to Pain States in Collagen-Induced Arthritis. *Arthritis & Rheumatology* 2015;67(6):1668-1677.
- [46] Nieto FR, Clark AK, Grist J, Hathway GJ, Chapman V, Malcangio M. Neuron-immune mechanisms contribute to pain in early stages of arthritis. *J Neuroinflammation* 2016;13(1):96.

- [47] Perrot S, Dieude P, Perocheau D, Allanore Y. Comparison of pain, pain burden, coping strategies, and attitudes between patients with systemic sclerosis and patients with rheumatoid arthritis: a cross-sectional study. *Pain medicine (Malden, Mass)* 2013;14(11):1776-1785.
- [48] Ruocco I, Cuello AC, Ribeiro-Da-Silva A. Peripheral nerve injury leads to the establishment of a novel pattern of sympathetic fibre innervation in the rat skin. *Journal of Comparative Neurology* 2000;422(2):287-296.
- [49] Seidah NG, Benjannet S, Pareek S, Savaria D, Hamelin J, Goulet B, Laliberte J, Lazure C, Chretien M, Murphy RA. Cellular processing of the nerve growth factor precursor by the mammalian pro-protein convertases. *The Biochemical journal* 1996;314 (Pt 3):951-960.
- [50] Selby MJ, Edwards R, Sharp F, Rutter WJ. Mouse nerve growth factor gene: structure and expression. *Molecular and Cellular Biology* 1987;7(9):3057-3064.
- [51] Sharif Naeini R, Cahill CM, Ribeiro-da-Silva A, Menard HA, Henry JL. Remodelling of spinal nociceptive mechanisms in an animal model of monoarthritis. *Eur J Neurosci* 2005;22(8):2005-2015.
- [52] Sharif Naeini R, Cahill CM, Ribeiro-da-Silva A, Ménard HA, Henry JL. Remodeling of spinal nociceptive mechanisms in a monoarthritis animal. *Eur J Neurosci* 2005;22(8):2005-2015.
- [53] Sofat N, Harrison A, Russell MD, Ayis S, Kiely PD, Baker EH, Barrick TR, Howe FA. The effect of pregabalin or duloxetine on arthritis pain: a clinical and mechanistic study in people with hand osteoarthritis. *Journal of Pain Research* 2017;10:2437-2449.

- [54] Sorge RE, Mapplebeck JC, Rosen S, Beggs S, Taves S, Alexander JK, Martin LJ, Austin JS, Sotocinal SG, Chen D, Yang M, Shi XQ, Huang H, Pilon NJ, Bilan PJ, Tu Y, Klip A, Ji RR, Zhang J, Salter MW, Mogil JS. Different immune cells mediate mechanical pain hypersensitivity in male and female mice. *Nature neuroscience* 2015;18(8):1081-1083.
- [55] Su J, Gao T, Shi T, Xiang Q, Xu X, Wiesenfeld-Hallin Z, Hokfelt T, Svensson CI. Phenotypic changes in dorsal root ganglion and spinal cord in the collagen antibody-induced arthritis mouse model. *The Journal of comparative neurology* 2015;523(10):1505-1528.
- [56] Suri S, Gill SE, Massena de CS, Wilson D, McWilliams DF, Walsh DA. Neurovascular invasion at the osteochondral junction and in osteophytes in osteoarthritis. *Ann Rheum Dis* 2007;66(11):1423-1428.
- [57] Tak PP. Is early rheumatoid arthritis the same disease process as late rheumatoid arthritis? *Best Practice & Research Clinical Rheumatology* 2001;15(1):17-26.
- [58] Walsh DA. *Arthritis pain; moving between early and late stage disease. Arthritis & rheumatology* (Hoboken, NJ) 2017.
- [59] Walsh DA, McWilliams DF. Mechanisms, impact and management of pain in rheumatoid arthritis. *Nat Rev Rheumatol* 2014;10(10):581-592.
- [60] Wu Z, Nagata K, Iijima T. Involvement of sensory nerves and immune cells in osteophyte formation in the ankle joint of adjuvant arthritic rats. *Histochemistry and cell biology* 2002;118(3):213-220.
- [61] Yen LD, Bennett GJ, Ribeiro-da-Silva A. Sympathetic sprouting and changes in nociceptive sensory innervation in the glabrous skin of the rat hind paw following partial peripheral nerve injury. *The Journal of comparative neurology* 2006;495(6):679-690.

Figure Legends

Figure 1. Intra-articular injection of CFA is associated with lasting pain-related behavior in male and female rats. Hind paw **A**, mechanical sensitivity, **B**, cold sensitivity scores **C**, heat hyperalgesia and **D**, ankle swelling. **E**, Ipsilateral static weight distribution following 20 minutes walking at 5.5m/min on a treadmill. Values are the mean \pm SEM (10 rats per group). * = $P < 0.05$, ** $P < 0.01$; *** = $P < 0.0001$ versus control, by two-way repeated-measure analysis of variance followed by Bonferroni corrected post-hoc t-tests (comparing timepoint to baseline except D where $p = \text{ipsi vs contra}$). (20 rats per group, except D where $n=12$, and E where $n=6$).

Figure 2. Significant changes to the cartilage are not detected until 4 weeks post-CFA injection. **A**, Toluidine blue staining of rat ankle joints like those used for quantification of joint changes shown in **B-E**. Black arrow points to the hypertrophic pannus, the boxes are enlarged in the images below in which the arrows point to blood vessels (with a blue overlay and grey outline for clarity) crossing the tideline (dotted line) where darkly stained non-calcified cartilage begins. Scale bar = 500 μm in the upper images, and 100 μm in the lower enlarged images. **B**, Number of vascularization points/mm of cartilage length in the talus and tibia. **C**, Thickness of the talus cartilage at the mid-point (μm). **D**, Optical density of toluidine blue staining of the cartilage. **E**, Scoring of damage to the cartilage. Bars represent the mean \pm SEM (6-10 male and female rats per group). * $P < 0.05$, ** $P < 0.01$; *** = $P < 0.001$ versus control, by two-way analysis of variance followed by Bonferroni corrected post-hoc t-tests.

Figure 3. Innervation of the skin adjacent to the CFA-treated joint is altered at 4 weeks. **A,** Identification of peptidergic nociceptors with anti-CGRP and sympathetic fibers with anti-DBH (dopamine beta hydroxylase) antibodies in contralateral and ipsilateral upper dermis and epidermis from the hindpaw adjacent to the ankle at 4 weeks post-CFA. The dotted line shows the dermal-epidermal junction, scale bar = 100 μm . The area within the white box is enlarged to the right and arrows point to where DBH and CGRP immunoreactive varicosities can be seen in close apposition to each other. Arrows point to fibers, scale bar = 25 μm (10 μm in enlargement). Note the finer looking fibers indicated by the unfilled arrow (filled arrow points to thicker fibers). **B.** Quantification of density of peptidergic fibers in the upper dermis and epidermis and sympathetic fibers in the upper dermis. Bars represent the mean \pm SEM (8-10 male and female rats per group), shown normalized to control. * = $P < 0.05$, ** $P < 0.01$; *** = $P < 0.001$ versus control, by paired t-tests. **C.** Sympathetic and peptidergic fibers in close apposition in the synovium at 4 weeks post-CFA, scale bar = 25 μm .

Figure 4. Glabrous skin is transiently inflamed. **A,** Detection of mast cells by metachromatic staining with toluidine blue in the upper dermis of the glabrous plantar skin adjacent to the ankle. Arrows point to mast cells, scale bar = 100 μm . Quantification of this is seen in **B**, bars represent the mean \pm SEM (10 male and female rats per group) *** = $P < 0.001$ versus control, by two-way ANOVA and post hoc t-tests. The organization of the skin appears altered in ipsilateral samples. **C,** A large inflammatory infiltrate in the hypodermis identified with CD68 immunoreactivity and toluidine blue staining. Dotted lines represent the boundary between the epidermis and upper dermis (upper dotted line), and between the upper and lower dermis (lower dotted line), scale bar= 100 μm . **D,** CD68 staining of cells associated with blood vessels in a region within the distal

talus at 4 weeks post-CFA; arrow points to a CD68 immunoreactive macrophage. Scale bar = 25 μ m. **E**, Mast cells in the synovium at 4 weeks post-CFA, scale bar = 50 μ m.

Figure 5. Innervation of the cartilage in CFA treated joints. **A**, Sympathetic fibers identified by VMAT2 immunoreactivity; in **Ai** note the morphology and presence of varicosities, associated with a vessel in the ipsilateral talus cartilage (red arrows). Dotted lines indicate the tideline at the osteochondral junction, with a chondrocyte indicated by a black arrow demonstrating that vessels and associated fibers are present in the cartilage. **Aii** shows grayscale images in **Ai**, to better show the overlay (here in red) drawn over the fibers as was used for quantification. **B**, Peptidergic fibers identified with CGRP immunoreactivity; note the morphology and the presence of varicosities, only in ipsilateral talus cartilage. Overlay shows blood vessels (light blue) and tideline (dotted line). In **Bii** blue arrows indicate fibers in the grayscale of images in **Bi**, note the blue overlay drawn over the fibers, similar to that used for quantification. Scale bar in A-Bi=50 μ m, in Bii=20 μ m. **C**, Quantification of fiber density as length per area (μ m/ μ m²) of sympathetic and peptidergic innervation of talus cartilage (n=4 male and female rats, extracted at 4 weeks post-CFA). Bars represent the mean \pm SEM, shown normalized to control.

Figure 6. NGF protein levels in **A**, synovial fluid extracted from the ankle joints, and from **B**, adjacent glabrous skin, with representative blots shown below (n=4-10 male and female rats, extracted at 4 weeks post-CFA). Bars represent the mean \pm SEM, shown normalized to control, ** P<0.01, ***P<0.001 Wilcoxon signed rank test, c= contra, i=ipsi, +=positive control of recombinant human NGF. Blots were cut and processed for proNGF and mNGF separately, denoted by the dotted line (loading controls can be found in the supplementary materials, available at <http://links.lww.com/PAIN/A967>).

Figure 7. In the dorsal horn, no change in nociceptor terminals was observed. Central terminals of peptidergic and non-peptidergic nociceptors detected by CGRP (magenta) immunoreactivity and IB4-lectin binding (green), respectively, in the contralateral and ipsilateral dorsal horn, scale bar = 200 μ m. Higher magnification images of single channels are shown in the side panels, scale bar = 100 μ m. Bars represent average intensity of staining (mean \pm SEM), normalized to contralateral values (n=9 male and female rats per group, extracted at 4 weeks post-CFA).

Figure 8. CFA-induced microgliosis but no astrocytosis **A**, Astrocytes were detected by GFAP immunoreactivity in the contralateral and ipsilateral dorsal horn. **B**, Quantification of the number and size of astrocytes (mean \pm SEM, n=8-10 male and female rats, shown normalized to contralateral). **C-D**, Microgliosis assessed by cell density and cell morphology with IBA1 staining in dorsal horns from sham, 2-week (2w) and 4-week (4w) post-CFA ipsilateral and 4-week post-CFA contralateral dorsal horns. Bars represent mean \pm SEM, *P<0.05, **P<0.01, by one way ANOVA with Bonferroni corrected t-tests, n=6-9 male and female rats, extracted at 4 weeks post-CFA. Scale bars = 100 μ m.

Figure 9. Markers of microglial activation are upregulated and expression of inhibitory terminals and KCC2 is reduced. Microglial markers CR3 (**A**) and CD68 (**B**) in contralateral and ipsilateral cords extracted at 4 weeks post-CFA. **C**, Bars represent mean \pm SEM of the average fluorescent intensity of the CD68 signal and the area occupied by CR3 staining in contralateral and ipsilateral dorsal horns, shown normalized to contralateral. *P<0.05, Mann-Whitney. ***P<0.001 by student's t-test (n=4-8 male and female rats). Scale bars=100 μ m **D**, Inhibitory terminals identified by VGAT (magenta) and KCC2 (green) immunoreactivity in contralateral and ipsilateral dorsal horns. Solid yellow line shows the dorsal boundary of the

dorsal horn and the dotted lines denote the limits of lamina I and lamina II respectively. Scale bar=50 μ m. **E**, Bars represent mean \pm SEM of the average fluorescent intensity VGAT and KCC2 signals in contralateral and ipsilateral dorsal horns, shown normalized to contralateral. *P<0.05, **P<0.01 by student's t-test (n=5-11 male and female rats). **F**, Downregulated KCC2 (green) and VGAT (magenta) in the ipsilateral cord can be seen together. Arrows point to KCC2 and VGAT on the cell membrane. Changes can be seen in inhibitory cells indicated by Pax2 (white) and excitatory cells (Pax2-; observed here in the ipsilateral images), note that no Pax2+ cells are visible in the contralateral fields. Arrowheads point to nucleoli, scale bar=10 μ m.

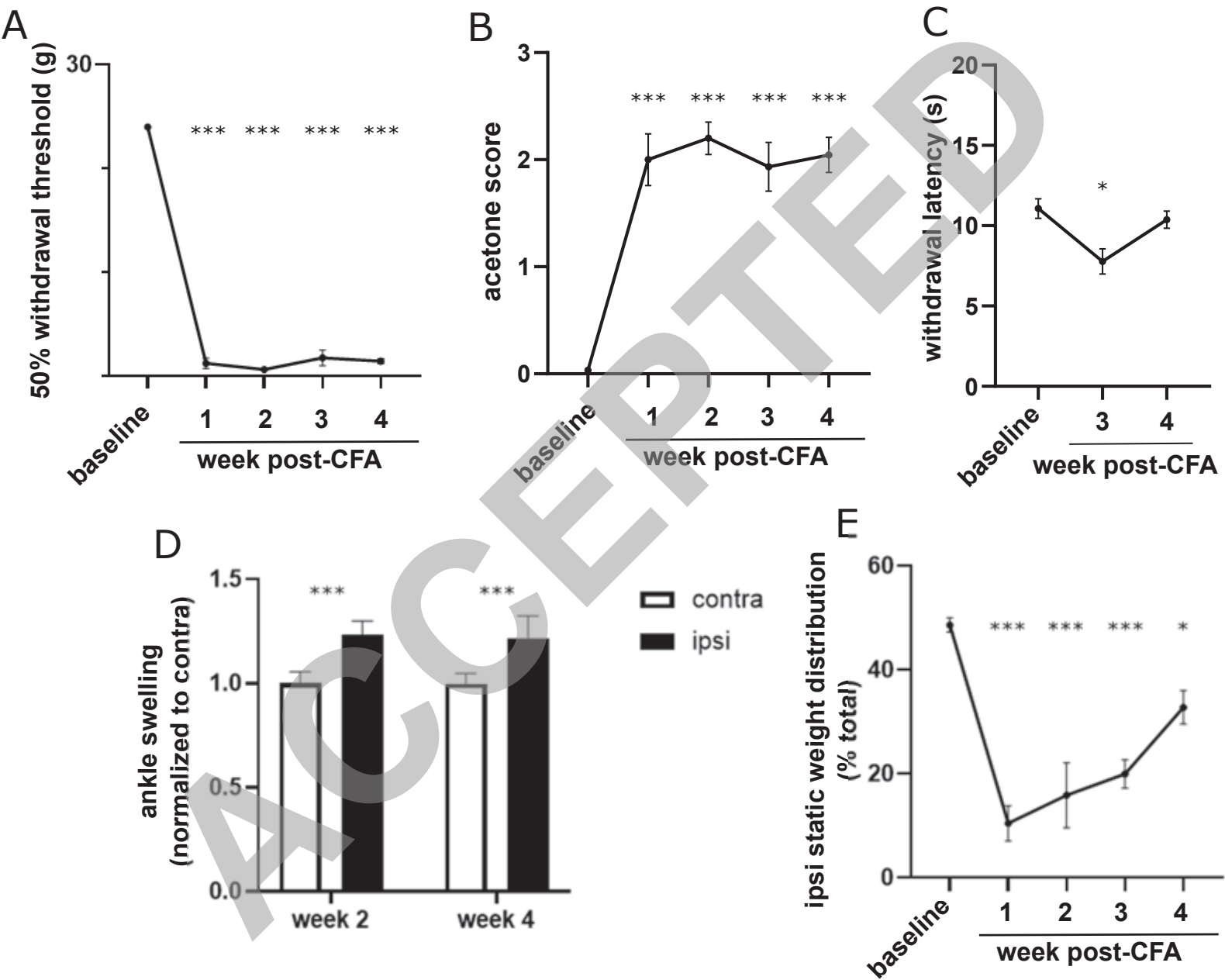


Figure 1

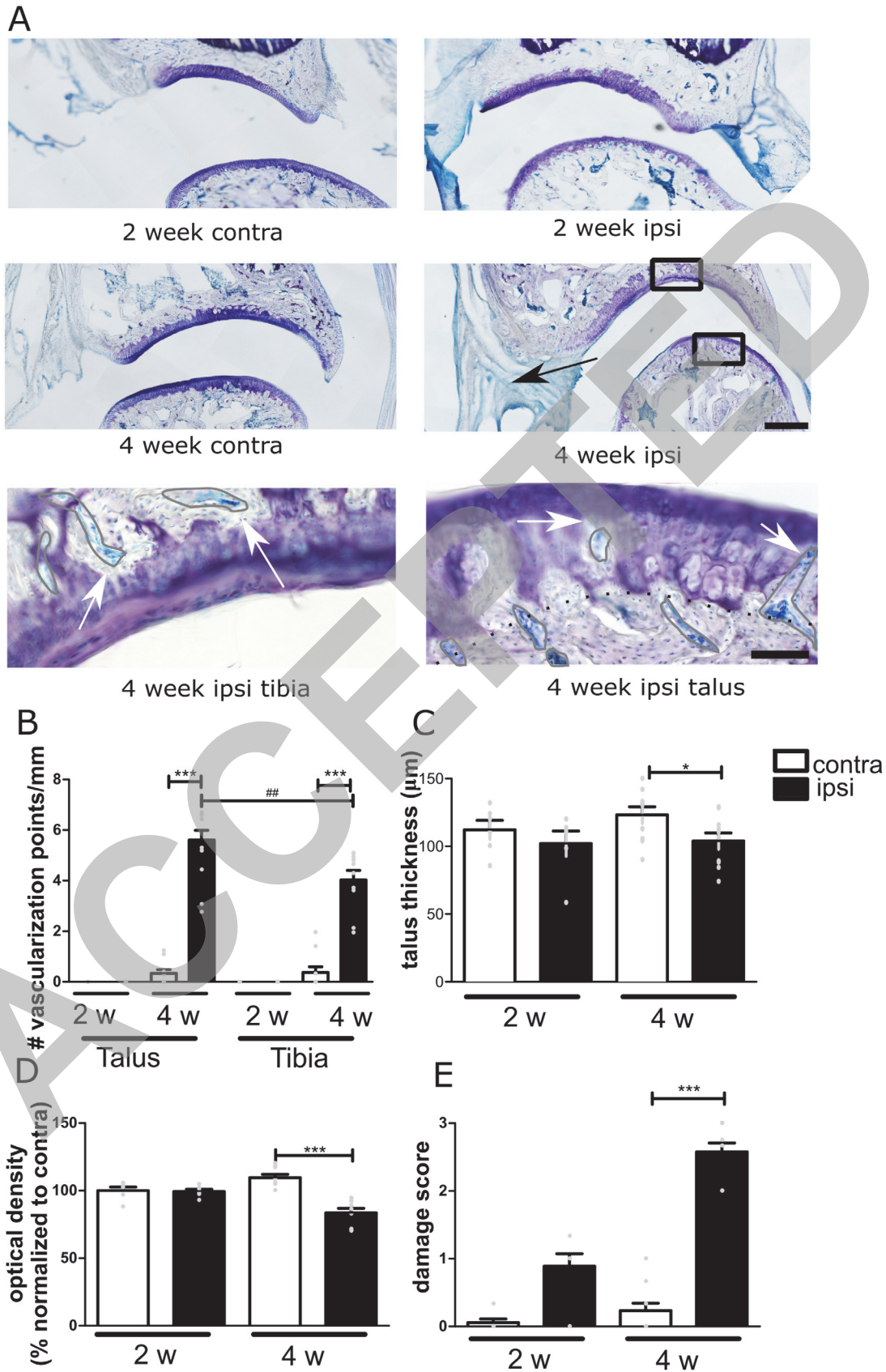


Figure 2

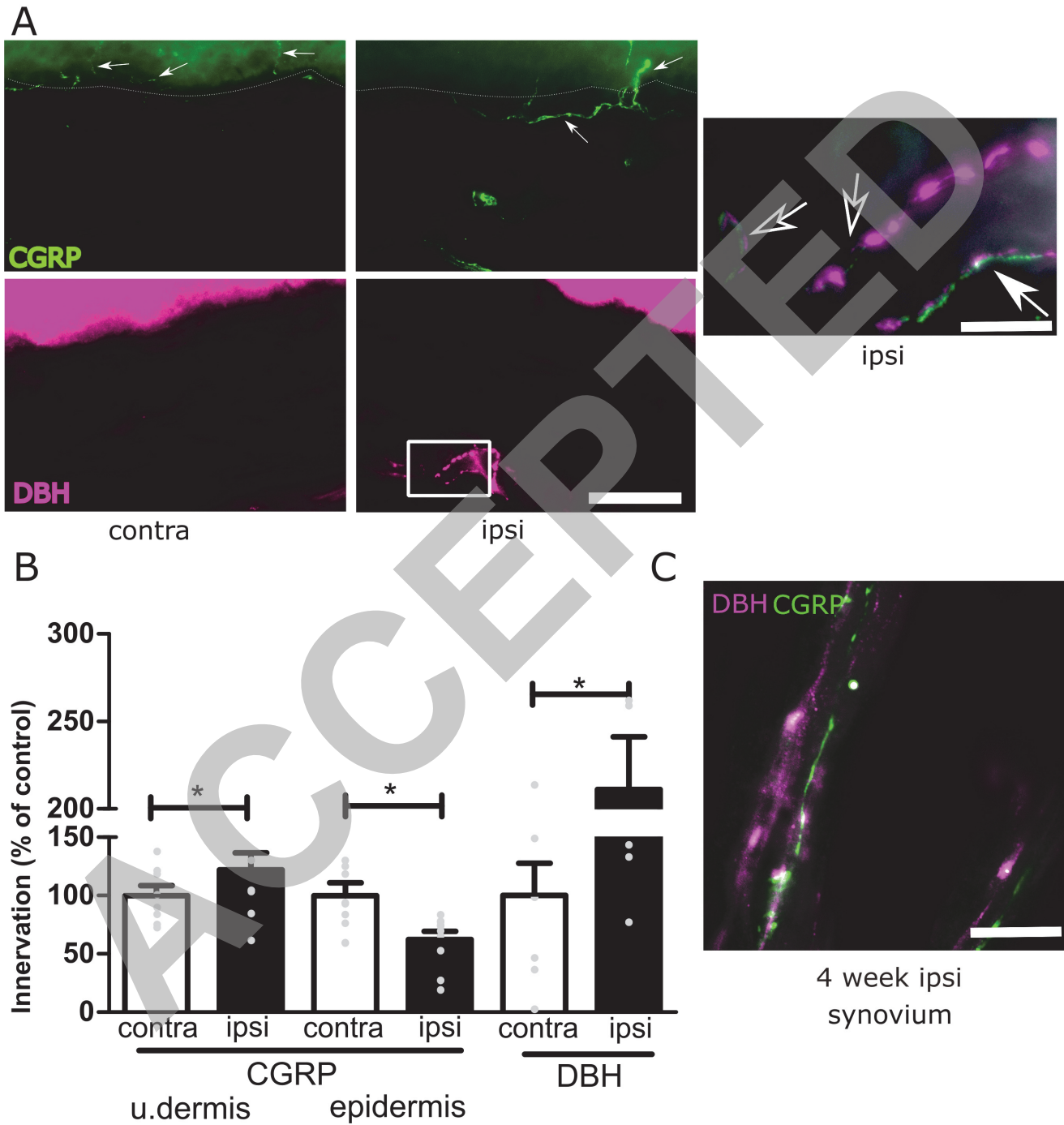


Figure 3

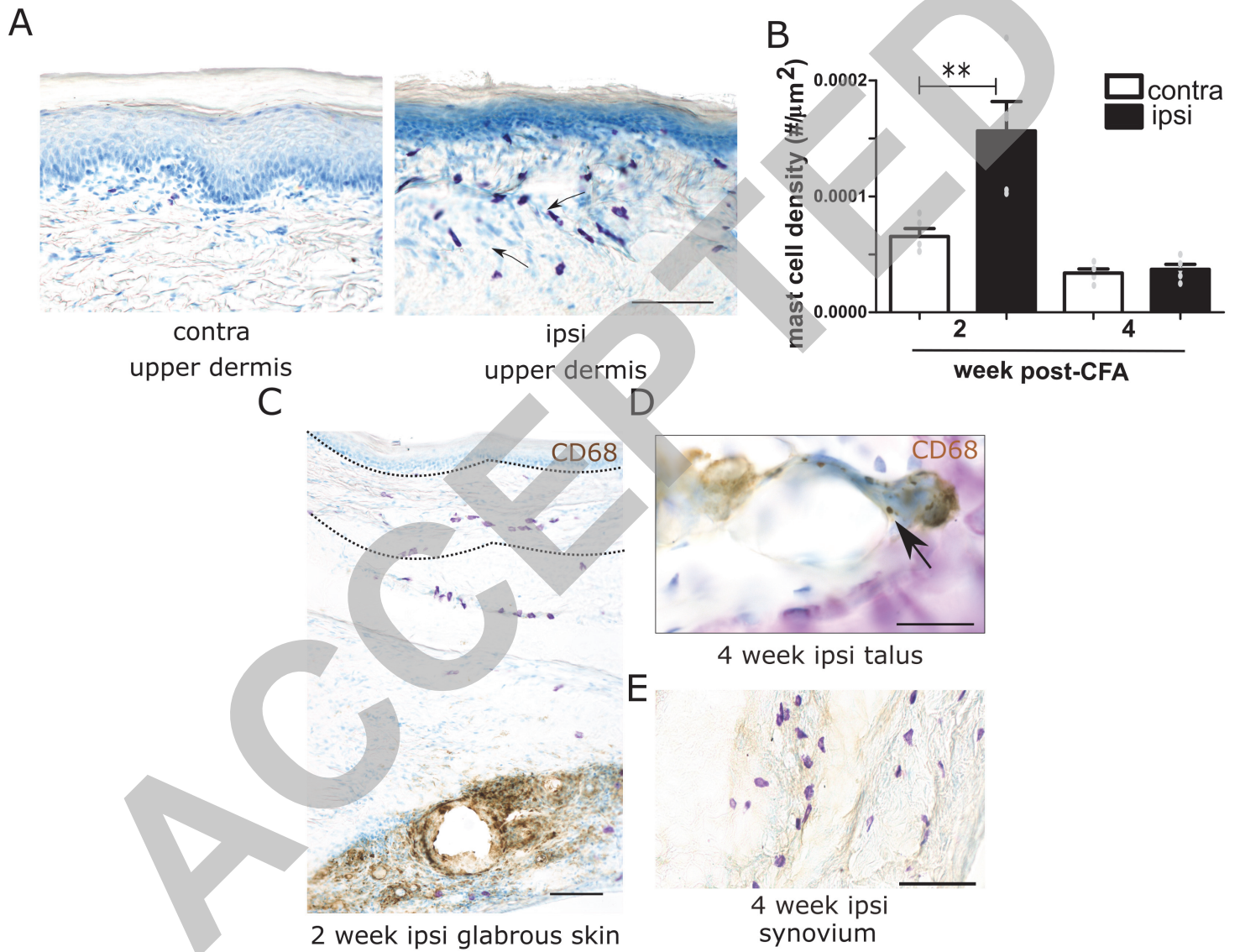


Figure 4

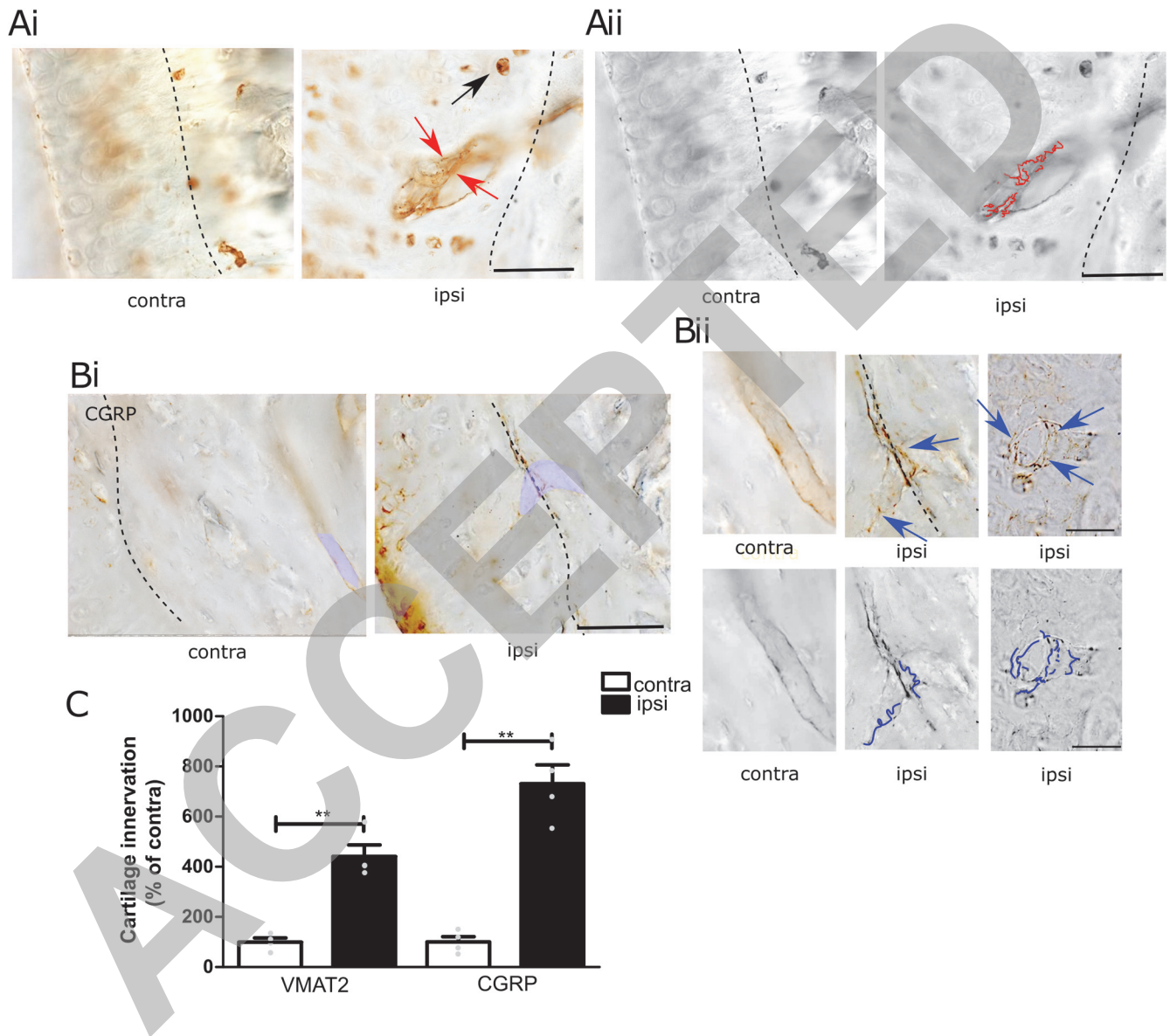


Figure 5

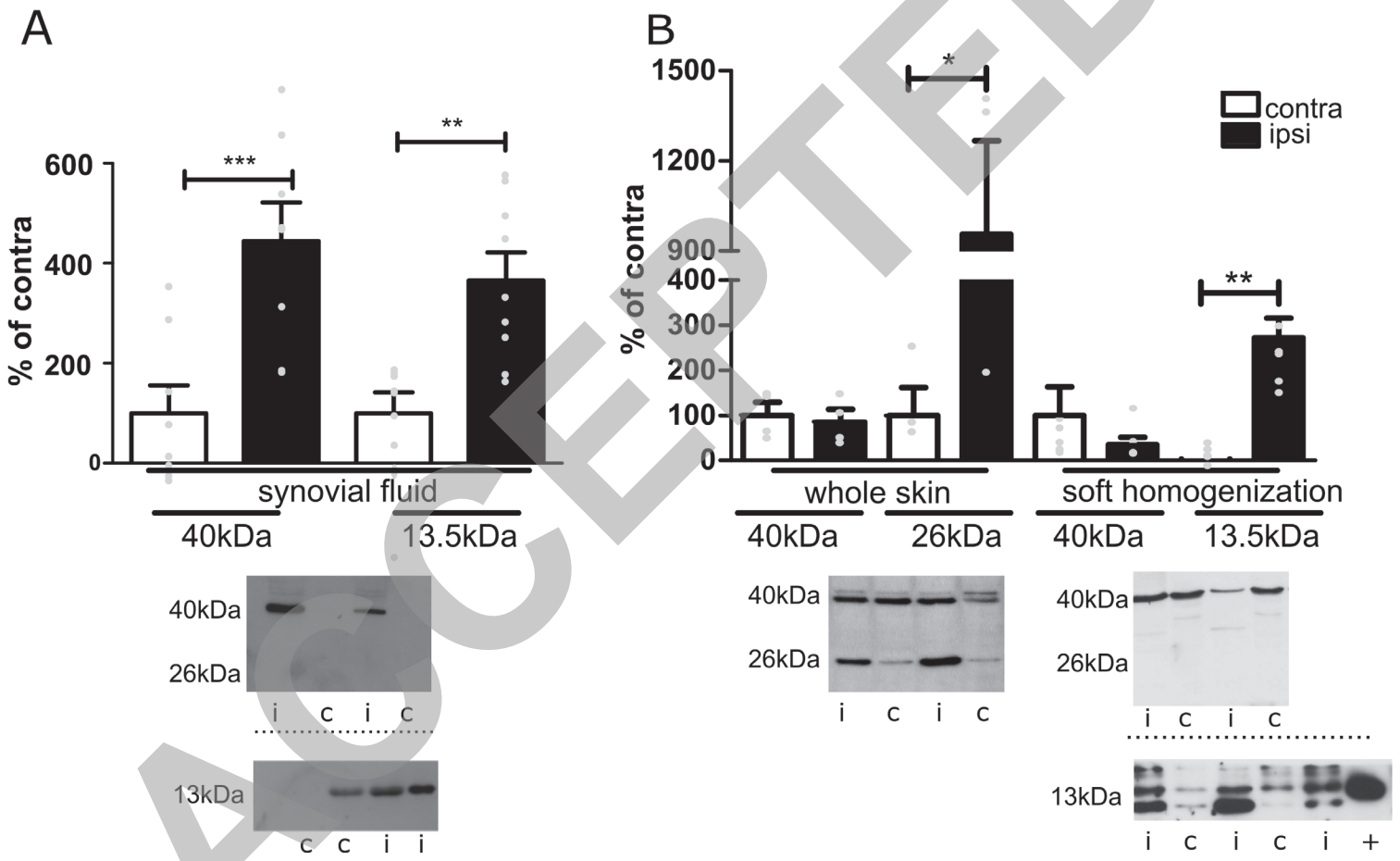


Figure 6

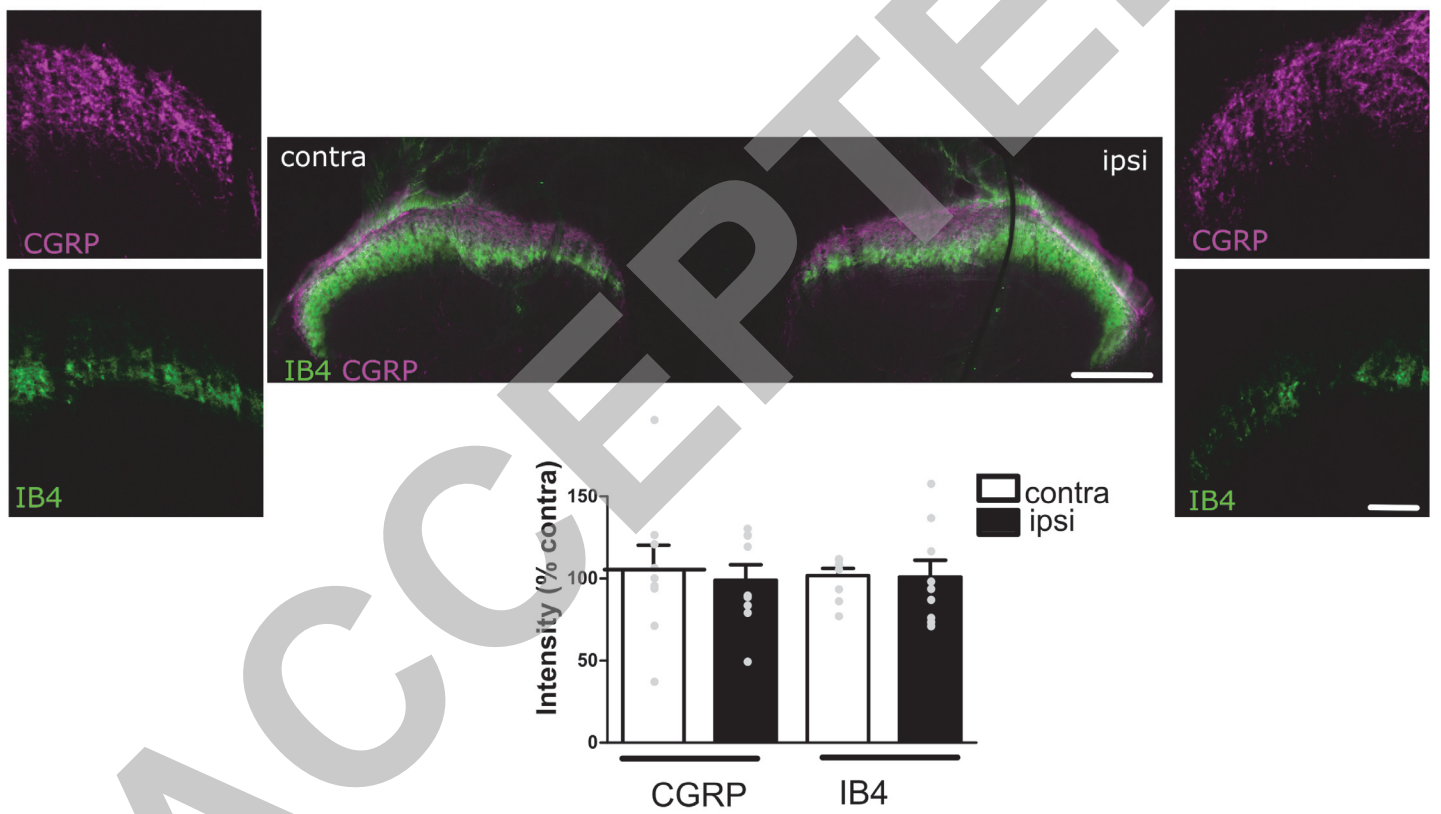


Figure 7

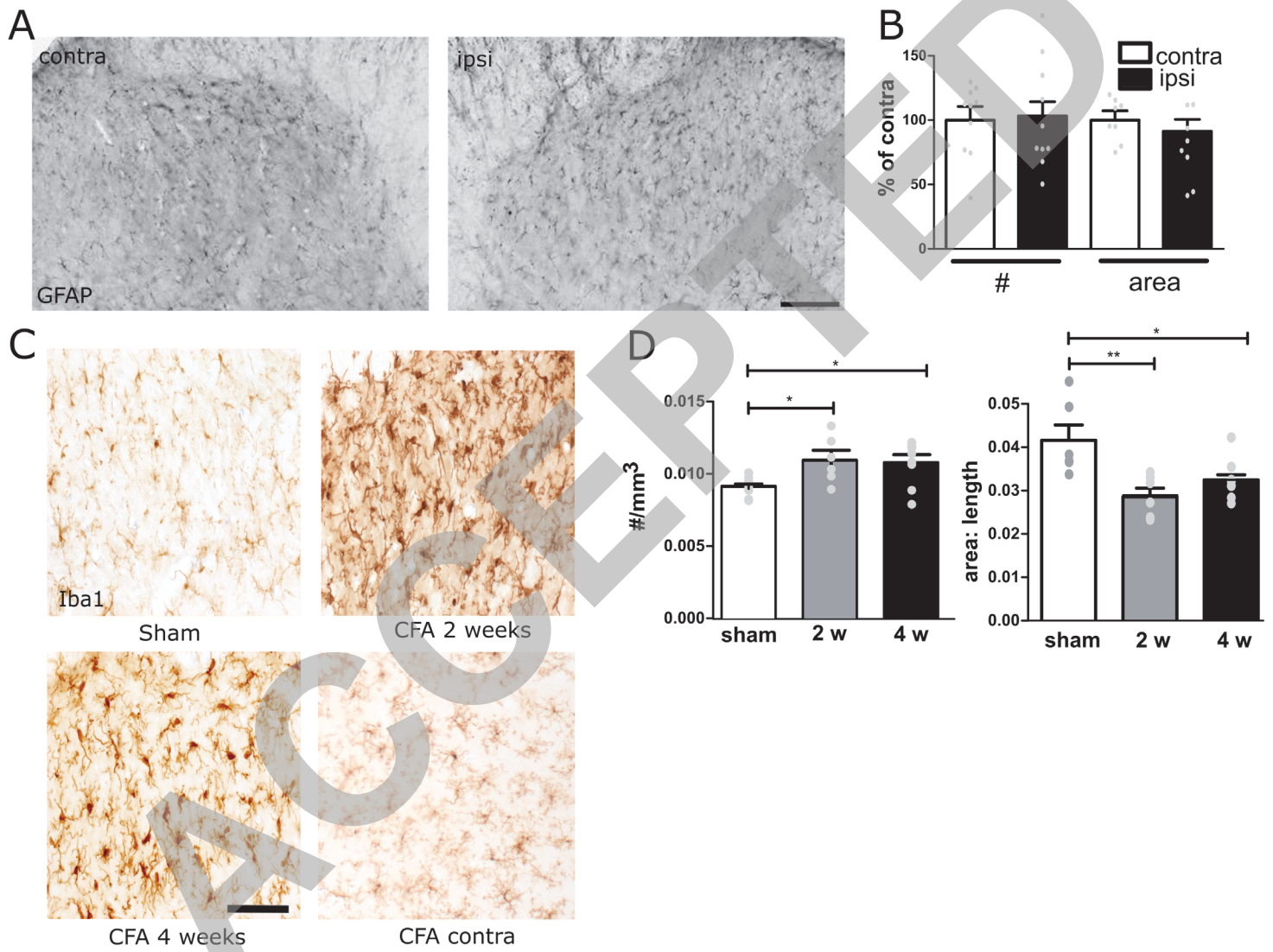


Figure 8

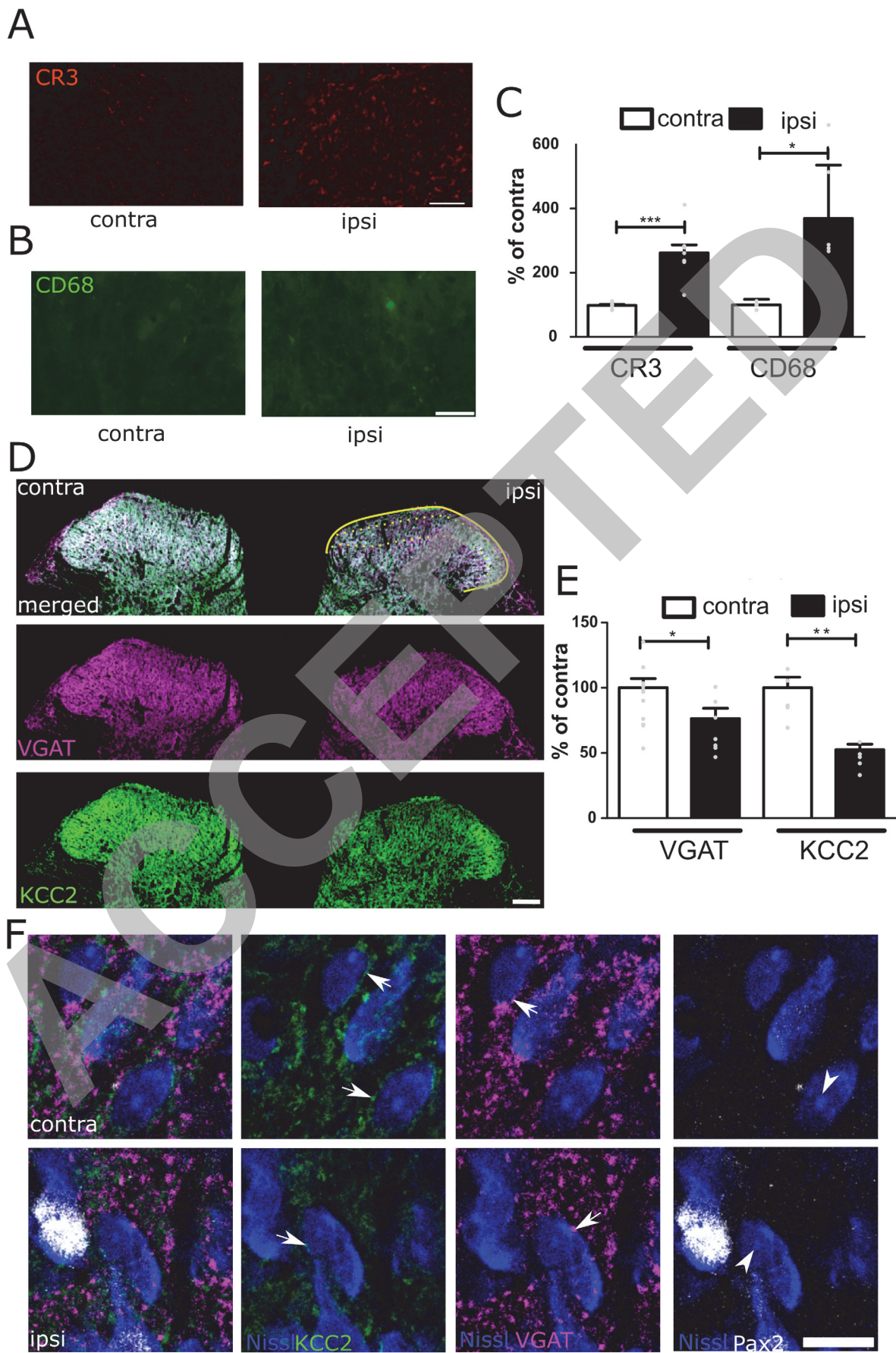


Figure 9